Migration velocity of red blood cells in microchannels

Sylvain Losserand, Gwennou Coupier, Thomas Podgorski

Migration velocity of red blood cells in microchannels

Sylvain Losserand, Gwennou Coupier, and Thomas Podgorski
Université Grenoble Alpes, CNRS, LIPhy, F-38000 Grenoble, France
(Dated: February 18, 2019)

The lateral migration of red blood cells (RBCs) in confined channel flows is an important ingredient of microcirculatory hydrodynamics and is involved in the development of a cell free layer near vessel walls and influences the distribution of RBCs in networks. It is also relevant to a number of lab-on-chip applications. This migration is a consequence of their deformability and is due to the combined effects of hydrodynamic wall repulsion and the curvature of the fluid velocity profile. We performed microfluidic experiments with dilute suspensions of RBCs in which the trajectories and migration away from the channel wall are analyzed to extract the mean behavior, from which we propose a generic scaling law for the transverse migration velocity valid in a whole range of parameters relevant to microcirculatory and practical situations. Experiments with RBCs of different mechanical properties (separated by density gradient sedimentation or fixed with glutaraldehyde) show the influence of this parameter which can induce significant dispersion of the trajectories.

INTRODUCTION

Blood is a dense suspension of essentially RBCs within plasma, which is a Newtonian fluid. RBCs have the particularity to be highly deformable in physiological conditions, which leads to complex flow patterns in confined environment due to several mechanisms.

One of the most famous features, first observed by Poiseuille [1], is the presence of a cell-free plasma layer (CFL) near vessels walls [2–6] inducing a decrease of the apparent viscosity referred to as Fåhræus-Lindquist effect [7] as well as a decrease of the hematocrit in small vessels compared to large ones [8, 9]. Several phenomena can be invoked to explain this cell free layer, one being geometrical: the presence of a capillary wall implies that the centers of RBCs must lie at least one RBC half-thickness away from the wall. This means that, on average, there will be more RBCs near the center of the capillary than very near the wall. The second one is hydrodynamical: at low-Reynolds number the deformability of RBCs allows a symmetry breaking that leads to transverse migration from the wall to the center of the channel [10, 11]. This symmetry breaking can also be obtained through the elastic deformation of the glycocalyx brush covering the endothelium [12]. Finally, RBC aggregation can have an influence on the CFL [5]. Transverse migration also plays a role in the so-called margination effect: contrary to RBCs which are concentrated around the centerline, other blood elements like white cells or platelets are marginated against the wall [13–19], which helps them to accomplish their function (e.g. in immune response, inflammation...). The centering of RBCs also influences the repartition of RBCs at bifurcations: due to the heterogeneity of the RBC concentration in vessels and the existence of a cell free layer, a heterogeneous distribution of the hematocrit takes place in the microcirculation [20–27].

The importance of understanding this migration is not limited to in vivo microcirculation but also has important possible applications in the design of Lab-on-Chip devices for particle separation. Geislinger et al. [28] presented a device capable to separate a dilute suspension of RBCs and platelets: the less deformable platelets migrate less than RBC and by controlling the position of the two outlets it is possible to separate the two populations. Important works are also done on a device named deterministic lateral displacement (DLD), which is made of a dense network of small pillars. The trajectory of particles inside this network is highly dependent on their properties, resulting in the possibility to separate different entities like RBCs [29], or different types of white cells [30].

In confined situations where the channel size is equal to a few cell radius, the effect of shape changes is strong and non-monotonous time variation of position can be observed. Numerical simulations explored the migration dynamics and the asymptotic position of simplified models of cells like 2D capsules [31] and 2D vesicles [32, 33] that can only qualitatively be compared to experiments. To date, although results are available on the shape and the position of RBCs in very confined channels [34, 35], there exist no experimental measurement and no quantification of migration dynamics of RBCs in confined Poiseuille flow (but in the pioneering work of Goldsmith [10]). The main objective of this paper is therefore to describe the migration of isolated RBCs for different confinements by using a simple general scaling law which could be used to validate numerical simulations, design future microfluidic devices or apply to some physiological situations where the hematocrit is low due to strongly heterogeneous distribution of cells at bifurcations in the microcirculation [20–27].

Transverse migration in simple shear flow

Among biomimetic models, giant vesicles are closed lipid membranes exhibiting in certain conditions, dynam-

ical properties that are similar to those RBCs, though they do not have cytoskeleton providing in plane shear elasticity. Their migration dynamics was theoretically described by Olla in [11]. For a vesicle with a fixed ellipsoidal shape, the drift velocity when the distance to the wall is large compared to vesicle size reads

$$\dot{y} = U\dot{\gamma}\frac{R_0^3}{y^2}, \tag{1}$$

where y is the distance of the center of mass to the wall, $\dot{\gamma}$ the shear rate of the unperturbed flow, R_0 the typical size of the vesicle and U a dimensionless parameter that depends on vesicle properties: the viscosity contrast λ between the inner and outer fluids and the reduced volume $\nu = 6\sqrt{\pi}\mathcal{V}/S^{3/2}$ where $\mathcal{V}$ is the vesicle volume and S its surface area. In the following, R_0 will be taken as the radius of the sphere of the same volume $\mathcal{V}$ as the considered particle: $R_0 = (3\mathcal{V}/4\pi)^{1/3}$. For RBCs of typical volume 90 µm^3 [36], this leads to $R_0 = 2.8$ µm.

This law has been confirmed later by 2D [37] or by 3D [38–40] numerical simulations and by theoretical analysis [40]. In the past years, several experiments in microgravity condition were conducted to measure this drift velocity [41, 42]. The overall scaling for the drift velocity as well as the value of the prefactor U are in agreement with simulations and theory (even though Olla assumes a fixed shape), for $\lambda = 1$ [39, 40] or higher values of λ [42]. Note that in Ref. [39] the $y^{-\alpha}$ scaling with $\alpha = 2$ seems to be valid for $y/R_0 \gtrsim 2$ and that for $1 \lesssim y/R_0 \lesssim 2$, α is smaller than 2, in agreement with the experimental near-wall study of Ref. [43] where $\alpha = 1$ is suggested.

Finally, similar y^{-2} scalings for the lift velocity were found for elastic capsules through numerical simulations [44, 45].

In physiological conditions, in terms of external fluid (plasma) viscosity and shear rates, isolated RBCs are far from a tank-treading regime [46–50] where they would adopt a fixed orientation relative to the flow. It was recently shown, however, that the scaling proposed for vesicles is still valid and a mean drift velocity (which corresponds to a drift velocity averaged over one body rotation period) characterized by $UR_0^3 = 0.36$ µm ^{3} was measured [51]. We are aware of no direct theoretical or numerical validation of this measurement.

Transverse migration in a channel

In a channel, the shear rate of the unperturbed flow is not uniform. This sole symmetry breaking is sufficient to induce migration of lipid vesicles even in the absence of walls [40, 52, 53]. In a realistic channel, wall lift and shear rate gradient contribute to migration in a complex way, in particular near the centerline where cell shape or dynamic depends a lot on its position close to this zero shear rate centerline. Over a wide range of confinement degree($2 < w/R_0 < 10$, where w is the half width of the channel), reduced volumes and viscosity ratios, it was shown experimentally in Ref. [54] that for lipid vesicles the migration velocity may be written as

$$\dot{y} = \xi\frac{R_0^{\delta+1}\dot{\gamma}(y)}{(y-y_w)^\delta}, \tag{2}$$

where δ is close to 1 and ξ a dimensionless parameter that depends on the vesicle properties, similar to U for the drift under simple shear rate and y_w is the position of the center of mass when the particle is as close as possible to the wall. For the quasispherical vesicles considered in [54], $y_w \sim R_0$ but in general, it may depend on particle deformability. This scaling was confirmed by 2D numerical simulations [54].

The alternative empirical law that we propose in this paper,

$$\dot{y} = \xi\frac{R_0^{\delta+1}\dot{\gamma}(y)}{y^\delta}, \tag{3}$$

is formally simpler and allows for comparison between different situations with no need to take into account the detail of the near-wall interactions. This formulation is the one generally used in the literature [11, 17, 55] and we shall consider it in the following. Indeed, RBCs are so deformable that y_0 can be very small and discussing its very precise value is not relevant from an experimental point of view, due to the dispersion in cell properties, initial cell orientation and the precision we can reach in its determination.

We show here that scaling law such as Eq. 3 can appropriately describe RBC migration in a confined channel and provide values for δ and ξ that are valid in a wide range of parameters.

EXPERIMENTAL SET-UP AND METHODS

The considered microfluidic channels are straight and of rectangular cross section. The width and the height of the section are respectively denoted $2w$ and $2h$, the useful length of the channel is 2.7 cm. RBCs flow along the Ox direction and migrate laterally along Oy. The walls are located at y=0 and $y = 2w$ in the Oy direction and at $z = -h$ and $z = h$ in the Oz direction (Fig. 1). Before the channel of interest, the flow is established over a long time resulting in a preliminary centering of the RBCs in the Oz direction ($z = 0$), depending on the width of the channel the preliminary centering in Ox is not necessarily complete. The suspension then reaches a T intersection: the control of the flow rate in the daughter branches permit to move the separation line, thus allowing to direct slightly more than the CFL of the incoming branch in

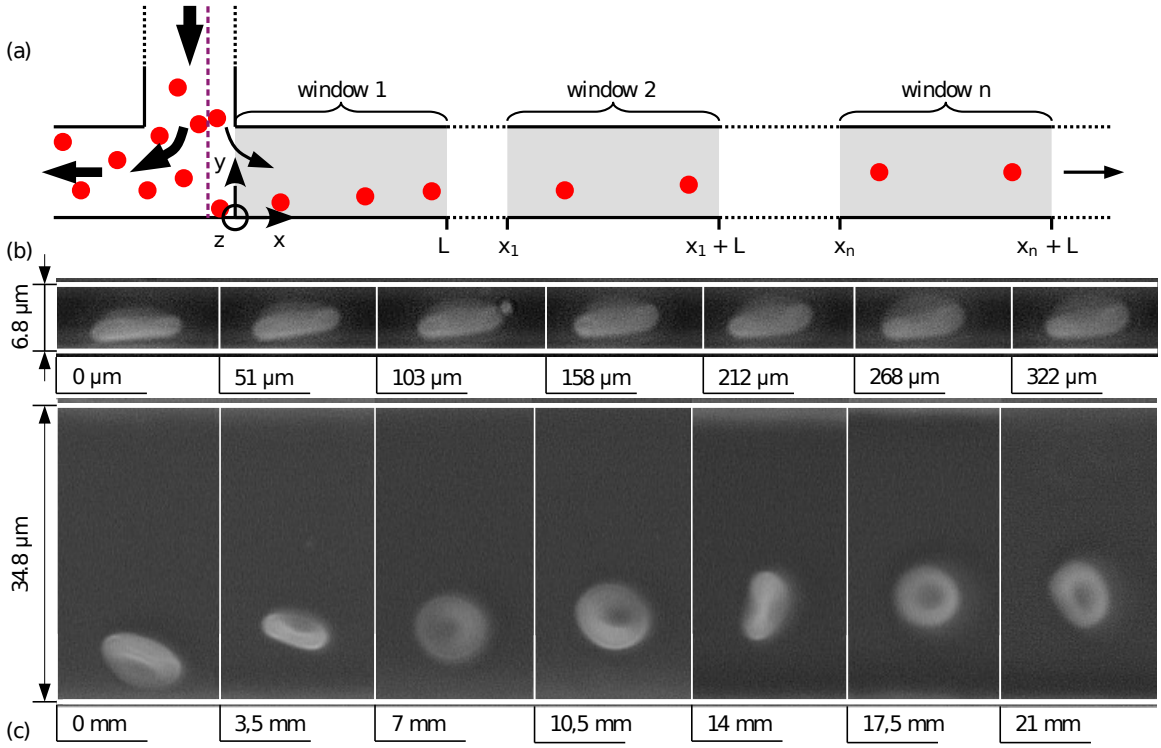

FIG. 1. (a) Sketch of the experimental channel. The separation line of the incoming flow is indicated by the violet dashed line. (b) Trajectory of a RBC migrating at high confinement (one single window). (c) Position of different RBCs in successive windows for a smaller confinement. RBCs are chosen to represent the median trajectory (see bottom middle panel in Fig. 4).

the outlet of interest and creating an initial condition where the incoming RBCs are near the wall ($y = 0$) in this outlet (Fig 1).

The channel is produced by soft lithography in polydimethylsiloxane (PDMS) bonded to a glass slide by plasma treatment. Channels with different sizes are used: w = 3.9, 6.2, 10.6, 12.5, 17.4, 27 µm with respective h = 4.8, 4.8, 6.5, 10, 10, 10 µm. The ratio between the characteristic channel size and the characteristic radius of the RBC (w/R_0) varies between 1.5 to 10. The flow is controlled thanks to a pressure controller (Elveflow™ Mk3).

Blood is supplied by the Etablissement Français du Sang (EFS) and is taken from healthy volunteers. Blood samples are first washed 3 times in a solution of phosphate-buffered saline (PBS tablet Sigma™: 10 M phosphate buffer, 2.7 M potassium chloride and 137 M with pH 7.4). Then samples are suspended at a low volume fraction (0.1%) so that RBC/RBC interactions become negligible in an isodense solution made of 70mL of Optiprep™ (iodixanol aqueous solution), 130mL of ultrapure water and a PBS tablet [56]. The buffer has a density of 1.112 ± 0.001 which prevents the sedimentation of the RBCs and a viscosity of $\eta_e = 1.9 \times 10^{-3}$ Pa s at 20°C which is a little higher than plasma viscosity (1.54 mPa s at 25°C [57]).

Furthermore, for one experiment, density-fractionated RBCs were prepared using discontinuous gradients with Optiprep. The gradient was built up in four layers of 2 mL, containing ultra pure water and respectively 40% (1.128 g mL^{-1}), 37% (1.118 g mL^{-1}), 33% (1.106 g mL^{-1}), 31% (1.099 g mL^{-1}) of Optiprep, buffered with a PBS tablet. 2 mL of blood sample initially washed using the method explained above are layered on the top of the gradient solution following a centrifugation at 3,000 rpm for 30 minutes at room temperature. After the centrifugation, two subpopulations are extracted and suspended in a density matched solution. The first population corresponds to RBCs having a density between 1.099 and 1.106 and represent the first $\simeq$ 5% of the total population, the second population has a density included between 1.118 and 1.128 representing the last $\simeq$ 10% of the total population.

Images are acquired with a 32X objective mounted on an inverted microscope (Olympus™ IX71) using a CMOS camera (ImagingSource™, DMK UX174) at a rate of 30 frames/s. RBCs are not followed directly, measurements are made on windows of size L=350 µm at different positions x; about 200 RBCs are observed by windows (see Fig. 1). A custom Python software using the library OpenCV™ [58] determines the center of mass of the projected shapes of RBCs. Using the trajectories of the RBCs obtained in each window, velocities $v_p(y, 0)$ are computed using a simple tracking program. Depending

on the confinement, the probability density function of the position y of the RBCs is calculated on a part or on the entire window. To reduce the influence of the outliers the median trajectory $y(x)$ is chosen to describe the trajectory of the RBCs. The dispersion y_d is defined as the mean between the position of the 33 $^{\text{rd}}$ and 66 $^{\text{th}}$ percentile. All lengths dimension are rescaled by w and are denoted with a $\sim$.

RESULTS

Longitudinal velocity — Fig. 2 shows the measured velocity v_p of RBCs as a function of their position $\tilde{y}$ (grey point). The maximum velocity is at $\tilde{y} = 1$ as for the fluid but the experimental plots show that v_p converges to 0 before $\tilde{y} = 0$. A straightforward explanation is the influence of the finite size of a particle compared to the size of the channel. There is no simple solution for this complex flow due to the presence of walls. Furthermore, the deformability and the complex shape of the RBC eliminate the possibility of a simple analytical solution.

A description of v_p is necessary in the continuation of this paper to translate the migration velocity (Eq. 3) into a description of the trajectory (Eq. 9). By considering RBCs as solid spheres, an analytical solution was proposed in 2D Poiseuille [59] flow but this approach cannot be easily extended to 3D flow. We approximated v_p by the mean velocity of the flow without RBC averaged on a square area of size $(2r)^2$ and of center of mass y and $z = 0$.

The mean velocity is thus written as an integral:

$$v_p(y,z) = \frac{1}{4r^2} \int_{z-r}^{z+r} \int_{y-r}^{y+r} v_x(Y,Z) dY dZ, \tag{4}$$

with v_x the velocity of the fluid without RBCs in a rectangular channel [60]:

$$v_x(y,z) = v_0 \sum_{n=1,3\ldots}^{\infty} a_n \left(1 - \frac{\cosh\left(b_n(y-w)\right)}{\cosh\left(b_n w\right)}\right) \cos\left(b_n z\right), \tag{5}$$

where

$$v_0 = \frac{v_{max}}{\sum_{n=1,3\ldots}^{\infty} a_n \left(1 - \frac{1}{\cosh\left(b_n w\right)}\right)}, \tag{6}$$

with $v_{max} = v_x(w,0)$ the maximal velocity of the fluid and

$$a_n = \frac{(-1)^{\frac{n-1}{2}}}{n^3},\ b_n = \frac{n\pi}{2h}. \tag{7}$$

This yields:

$$v_p(y,z) = v_0 \frac{h}{\pi r^2} \sum_{n=1,3\ldots}^{\infty} \frac{a_n}{n} \sin\left(b_n r\right) \left(r - \frac{\sinh\left(b_n r\right)\cosh\left(b_n(y-w)\right)}{b_n \cosh\left(b_n w\right)}\right). \tag{8}$$

Despite our rough assumption, the fit using Eq. 8 with v_{max} as a free parameter and $r = R_0$, gives a correct approximation of the experimental values (see Fig. 2). The model brings to light the effect of the confinement on the difference between v_p and v_x: an increase of the channel width induces a reduction of the difference between the two velocities. Discrepancies with the model appear near the wall and come from the fact that the model does not take into account the non negligible influence of the RBC on the flow. This influence being stronger near walls, the discrepancies should be stronger near walls as shown by Goldman [61]. v_{max} obtained from the fit using Eq. (8) is between 0.5 and 3 $\mathrm{mm\,s^{-1}}$ which is in the range of typical values observed in microcirculation. A capillary number $Ca = \eta_e \dot{\gamma}_e R_0/\mu_s$ can be introduced, with $\dot{\gamma}_e = v_{max}/w$ a characteristic shear stress and $\mu_s = 3$ $\mathrm{\mu N\,m^{-1}}$ for the RBC shear elasticity [62]. Ca is found to be between 1 and 7.

Transversal velocity — Fig. 3 shows an experimental result for $w = 10.6$ µm. RBCs move away from the wall and migrate towards the center. Eq. 3 describes the migration velocity and from this equation the theoretical trajectory $y_{th}(x)$ obeys the differential equation:

$$\frac{\partial y_{th}}{\partial x} = \xi \frac{R_0^{\delta+1} \dot{\gamma}(y_{th},0)}{y^{\delta}\ v_p(y_{th},0)}. \tag{9}$$

$\dot{\gamma}$ and v_p are respectively obtained from Eq. 5 and Eq. 8. Both expressions are proportional to v_{max}, therefore the trajectory does not explicitly depend on v_0. Consequently, the potential inaccuracies in its determination through the cell velocity will not affect the determination of the lift parameters. The data are fitted using Eq. 9. A first step consists in integrating it numerically and in a second step the residual of a cost function is computed. The problem has three free parameters ξ, δ and the initial value of y denoted y_0. The minimization of $< |(\tilde{y} - \tilde{y}_{th}/\tilde{y}_d| >$ is based on a global method named differential-evolution [63]. In Fig. 3 different fits of the same dataset are shown, all of them giving reasonable results. The value of y_0 found from minimization is pretty constant and appears to be independent of the two other parameters. In contrast, δ and ξ seem correlated as an increase of one induces the increase of the other one.

By fixing $\tilde{y_0} = \tilde{y}(0)$, the residual can be explored in the (δ, ξ) parameter space, as shown in the insert of Fig.

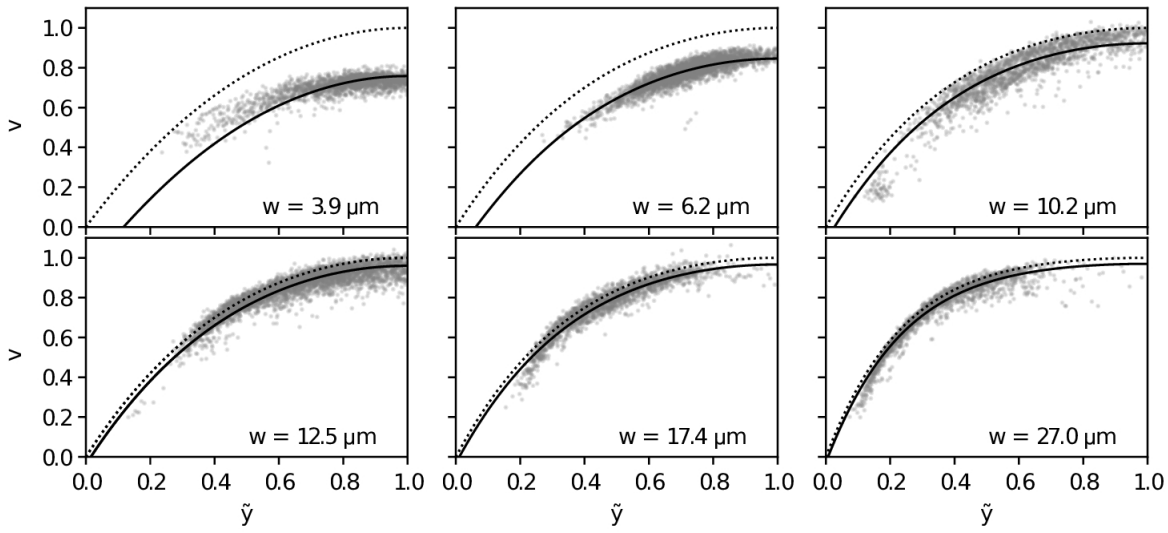

FIG. 2. Grey points: measured velocity of RBCs, rescaled by v_{max} from Eq. (6) which is obtained from the fitting of experimental data using Eq. (8). The dashed line represents the velocity of the fluid v_x without RBC at $z = 0$ using Eq. (5) and the full line represents the fitted velocity using Eq. (8).

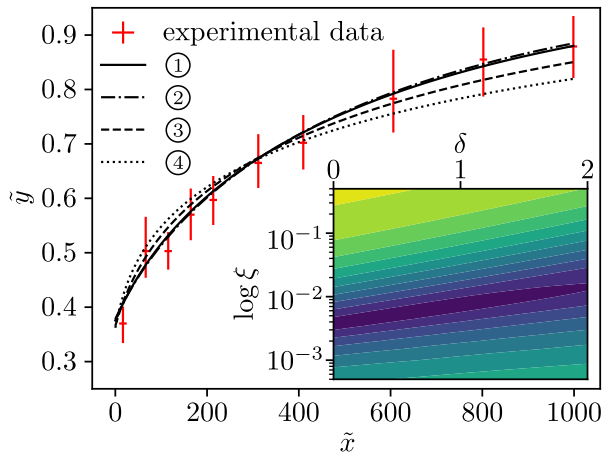

FIG. 3. Trajectory of RBCs in a channel with $w = 10.6$ µm (red). Fitting curves (black) using different couples of parameters (δ, ξ, y_0), in ① all parameters are free, giving at the end (0.14, 4.1×10^{-3}, 0.38), ②, ③, ④ are fits using a fixed δ giving respectively (0, 3.7×10^{-3}, 0.38), (1, 7.7×10^{-3}, 0.37), (2, 1.6×10^{-2}, 0.36). The surface plot in insert shows the residual $\sum |(\tilde{y} - \tilde{y_{th}})/\tilde{y_d}|$ in the (δ, ξ) parameter space. Dark blue color represents the minimal residual.

3. The blue zone corresponds to $< |(\tilde{y} - \tilde{y}_{th}/\tilde{y_d}| > \leq 0.5$. Thus parameter values (δ, ξ) present in this zone give an error inferior to y_d. This zone varies from confinement to confinement and no clear law relating the 2 parameters can be extracted. In more simple geometry [51] or with simpler objects [41, 42, 54], these two parameters were instead shown to be independent of each other. We consider here that the apparent correlation for a given confinement is the result of the specific migration function combined with the noise in the data that prevents a more accurate fit. Aiming at finding a (δ, ξ) couple of values that gives the best fit over a wide range of parameters, we thus take into account the whole set of results in different channels. For each experiment, for a fixed value of $y_0 = y(0)$ and δ ranging from 0 to 2 with a step of 0.05, the value of ξ minimizing the residual is determined. By considering all the channels a mean $< \xi >$ and a normalized mean square error $\Delta\xi = \sqrt{< (\xi - < \xi >)^2 >}/ < \xi >$ as a function of δ can be computed. From the minimum of the mean square error (see Fig. 4, top left) we extract the most probable value for δ and ξ: $\delta_s = 1.30 \pm 0.05$ and $\xi_s = 1.1 \times 10^{-2} \pm 0.2 \times 10^{-2}$.

The RBC trajectories $\tilde{y}(\tilde{x})$ are shown in Fig. 4 for five different confinements. In our range of parameters, RBCs move from the wall towards the center of the channel in agreement with the results of [34] and the migration velocity decreases as RBCs approach the centerline. The fit obtained from (3) with $\delta = \delta_s$, $\xi = \xi_s$ and y_0 free give good results even at high confinement where the lateral migration is mainly the result of the deformation of the RBC.

We also investigatde the influence of RBC mechanical properties by isolating the most and less dense fractions of RBCs in a density gradient (see Experimental Set up and Methods). Fig. 5 shows that less dense RBCs migrate faster than denser RBCs, the comparison of their respective ξ obtained from the fit of Eq. (9) when $\delta = \delta_s$ is fixed show a clear difference: 1.4×10^{-2} for the less dense and 6.5×10^{-3} for the denser ones. Denser RBCs are usually considered more aged than less dense RBCs [64]. Different interpretations can be found

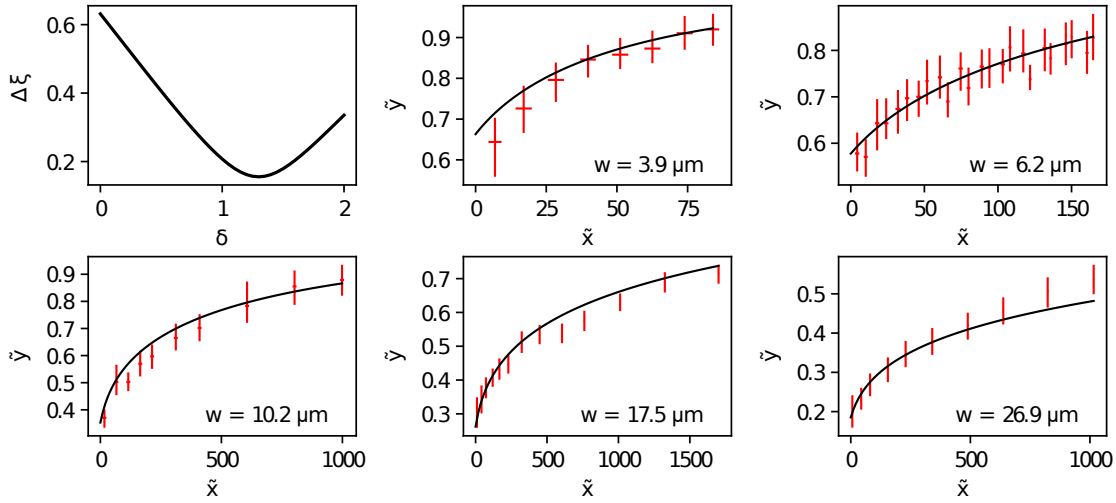

FIG. 4. Top left: mean square error $\Delta\xi$ as a function of δ. Other plots represent the median trajectory $\tilde{y}(\tilde{x})$ of RBCs for 5 different confinements (red) and their respective fitting curves (black) found from Eq. (9) using fixed δ_s and fixed ξ_s with $\tilde{y}_0$ a fitting parameter.

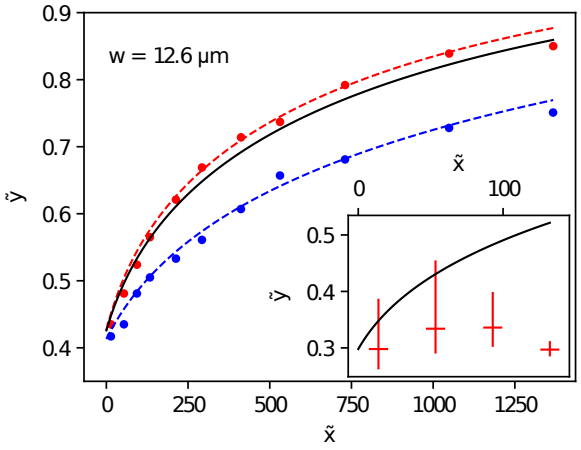

FIG. 5. Fit of experimental data for the lift in Poiseuille flow (channel size of 25μm) of two different populations of RBCs. The red color represents the median trajectory of the less dense RBCs (points) and its fitting curve using Eq. (9) with a fixed δ_s, free ξ and $\tilde{y_0}$ (dashed line). The blue color denotes the trajectory and its respective fit for the denser RBCs. The black curve is the general trajectory found previously using δ_s and ξ_s and $\tilde{y_0}$ the mean between $\tilde{y}(0)$ of the two experimental curves. The insert represents the median trajectory of rigidified RBCs in red and the general trajectory in black.

in the literature about the effect aging on RBCs, either through a dehydration of RBCs that leads to an increase of hemoglobin viscosity, or to modification of membrane properties [65, 66]. Netherless, there are strong indications that older cells have a higher density and lower deformability [67] (eventually leading to their elimination in the spleen [68]). Our study also indirectly suggests that denser cells are less deformable.

For comparison, the insert in Fig. 5 shows that artificially hardened RBCs using glutaraldehyde (at a concentration $> 0.1\%$ so that proteins are completely crosslinked and RBCs become rigid [69]) lose their capability to migrate and behave like rigid particles. The deformability is thus an important parameter in the migration dynamics.

DISCUSSION

An exponent different from $\delta = 2$ may be interpreted in several ways. Except when the vesicle is close to the center, its migration velocity in an unbounded Poiseuille flow is constant ($\delta = 0$). An exponent between 0 and 2 might be seen as a kind of average between the contributions of wall-induced lift and migration due to non-constant shear rate. Still, the weight of these contributions is not the same depending on the position of the particle [70, 71], so it is not clear whether such a scaling with a δ exponent independent from the cell radius to channel size ratio would hold.

In Ref. [17], 3D RBCs were simulated in a 2D Poiseuille flow; the cells' membrane have the same properties as that of red blood cells but the viscosity of the inner fluid is taken to be equal to that of the external fluid. In addition, the capillary number is quite large such that the dynamics of the cells resembles that of vesicles, with tank-treading like motion accompanied by some small oscillations. They find that for a channel width of 12 and 18 cell radius, a scaling law such as Eq. 3 is found with δ in the range 1.2-1.3 on average, with ξ in the range

0.04-0.07. We thus find a similar range for δ, but smaller values for ξ. This may be explained by the value of the viscosity contrast, which is not 1 in reality. Increasing the viscosity contrast generally leads to a decrease of ξ in Poiseuille flow [54] or of U in simple shear flow [11, 42]. In Ref. [51], we found a factor 9 for the U values between the physiological case and a viscosity contrast close to 1. The similarity in the range for δ shows that the found values well describe the interplay between wall and shear gradient effects, in that range of confinement. To the contrary, our results are in contradiction with the model proposed in [18]: it is proposed that because of shape change with the shear rate, therefore with the y position, ξ may also depend on y [18]. This may somehow be transcripted into a different exponent δ, as long as the migration velocity is confronted to numerical or experimental data that spans on a limited range and/or are associated with noise. In Ref. [18], δ is set to 2 and the proposed modeling implies that ξ is a decreasing function of y, which implies that the velocity decreases much more strongly with y then in Eq. 3 with ξ constant and $\delta \sim 1.3$.

The structure of a RBC suspension is the result of two counterbalancing effects, lift and multiple collisions between cells, that lead to transverse diffusion [51]. This controls in particular the width of the cell free layer near the walls.

In Ref. [18], a good agreement with the literature is found for the gap size for a suspension simply sheared between two walls, using two approaches: direct numerical simulations of cells, or a theoretical approach solving the lift+diffusion equation. The simulations are run with elastic capsules whose mechanical properties are such that they are essentially in a tank-treading regime. Agreement with the theory is obtained by considering a fitting parameter U/f of order 0.5, where U is the dimensionless prefactor of Eq. 1 and f that of the diffusive flux written as $-fR_0^2\dot{\gamma}\Phi\frac{\partial\Phi}{\partial y}$. This makes sense, since this value of the parameter is quite close to that obtained for lipid vesicles in tank-treading regime: in [41] we found U to be of order 0.1 and in [42] f is shown to be of order 0.06, which makes $U/f \sim 1.7$. It was also argued in [18] that the crowded environment in which these interactions take place justify to consider an effective viscosity of the carrying fluid higher than that of the plasma. Indeed, from [51], one can see that for RBCs in plasma, $U/f_2 \simeq 0.016/2.8 \simeq 0.006$, which would certainly not be sufficient to create a cell free layer. Of course, it is clear that a cell lifting in a crowded environment will not lift the same way as an isolated cell, because the neighbors may modify its dynamics and response to flow, and will screen the wall. Considering tank-treading capsules for mimicking the collective behavior of red blood cells as in [18] or [17] appears thus as relevant for obtaining accurate predictions, though the choice of the effective viscosity contrast must be debated, as in Ref. [3]. Still, it hides the subtle modification of lift mechanisms by cell-cell interaction processes.

By dimension analysis in a 2D Poiseuille flow, it is possible to estimate a typical time describing the time needed for RBC to migrate frome the wall ($y = 0$) to the distance corresponding to the CFL ($y = d$) :

$$\tau_L = \frac{w d^{\delta_s+1}}{v_{max}\xi_s R_0^{\delta_s+1}}. \tag{10}$$

Shear-induced diffusion also contributes to equilibration, with an equilibration time deduced from the expression of the diffusive flux below,

$$\tau_D = \frac{w^3}{f v_{max}\Phi_0 R_0^2}, \tag{11}$$

where Φ_0 is a typical volume fraction in cells.

Using results from Fedosov [2], for a channel of typical size $w = 5$ µm, with $\Phi_0 = 30\%$ and a CFL of size $d = 2$ µm, the distance needed for all RBC to pass through the CFL is $\tau_L v_{max} = 200$ µm and the one to obtain an equilibration is $\tau_D v_{max} = 150$ µm. The found typical distances are of the same scale and indicate that, in the microcapillary network, except in the smalles capillaries, equilibration is not likely to happen between two successive bifurcations, which are often very close to each other. [1, 26, 72, 73]. Non stationary dynamics must, therefore, be considered when looking at network flow. The factor 2 that we found in the ξ values for the denser (less deformable) and less dense (more deformable) cells also indicates that uneven distribution of cells depending on their age may also occur in the microvasculature.

ACKNOWLEDGMENTS

This work was partially supported by CNES (Centre National d'Etudes Spatiales). The authors' team is part of LabEx Tec 21 (Investissements d'Avenir - grant agreement ANR-11-LABX-0030). S. L. thanks LabEx Tec 21 for a Proof of Concept fellowship.

[1] J.-M. Poiseuille, Comptes rendus hebdomadaires des séances de l'Académie des sciences **1**, 554 (1835).
[2] D. A. Fedosov, B. Caswell, A. S. Popel, and G. E. Karniadakis, Microcirculation **17**, 615 (2010).
[3] V. Narsimhan, H. Zhao, and E. S. G. Shaqfeh, Phys. Fluids **25**, 061901 (2013).
[4] D.Katanov, G. Gompper, and D. A. Fedosov, Microvasc. Res. **99**, 57 (2015).
[5] J. M. Sherwood, J. Dusting, E. Kaliviotis, and S. Balabani, Biomicrofluidics **6**, 024119 (2012).
[6] S. Yamaguchi, T. Yamakawa, and H. Niimi, Biorheology **29**, 251 (1992).

[7] R. Fåhræus and T. Lindqvist, Am. J. Physiol. **96**, 562 (1931).
[8] R. Fåhræus, Physiol. Rev. **9**, 241 (1929).
[9] A. S. Popel and P. C. Johnson, Annu. Rev. Fluid Mech. **37**, 43 (2005).
[10] H. L. Goldsmith, Fed. Proc. **30**, 1578 (1971).
[11] P. Olla, J. Phys. II France **7**, 1533 (1997).
[12] H. S. Davies, D. Débarre, N. El Amri, C. Verdier, R. P. Richter, and L. Bureau, Phys. Rev. Lett. **120**, 198001 (2018).
[13] H. L. Goldsmith and S. Spain, Microvasc. Res. **27**, 204 (1984).
[14] A. Kumar and M. D. Graham, Phys. Rev. Lett. **109**, 108102 (2012).
[15] D. A. Fedosov, J. Fornleitner, and G. Gompper, Phys. Rev. Lett. **108**, 028104 (2012).
[16] M. Mehrabadi, D. N. Ku, and C. K. Aidun, Phys. Rev. E **93**, 023109 (2016).
[17] Q. M. Qi and E. S. G. Shaqfeh, Phys. Rev. Fluids **2**, 093102 (2017).
[18] R. G. Henríquez Rivera, X. Zhang, and M. D. Graham, Phys. Rev. fluids **1**, 060501 (2016).
[19] C. Bächer, A. Kihm, L. Schrack, L. Kaestner, M. W. Laschke, C. Wagner, and S. Gekle, Biophysical Journal **115**, 411 (2018).
[20] B. M. Fenton, R. T. Carr, and G. R. Cokelet, Microvascular Research **29**, 103 (1985).
[21] A. R. Pries, K. Ley, M. Claassen, and P. Gaethgens, Microvasc. Res. **38**, 81 (1989).
[22] J. O. Barber, J. P. Alberding, J. M. Restrepo, and T. W. Secomb, Ann. Biomech. Eng. **36**, 1690 (2008).
[23] V. Doyeux, T. Podgorski, S. Peponas, M. Ismail, and G. Coupier, Journal of Fluid Mechanics **674**, 359388 (2011).
[24] Z. Shen, G. Coupier, B. Kaoui, B. Polack, J. Harting, C. Misbah, and T. Podgorski, Microvasc. Res. **105**, 40 (2016).
[25] S. Roman, A. Merlo, P. Duru, F. Risso, and S. Lorthois, Biomicrofluidics **10**, 034103 (2016).
[26] P. Balogh and P. Bagchi, Phys. Fluids **30**, 051902 (2018).
[27] E. Kaliviotis, J. Sherwood, and S. Balabani, Scientific reports **7**, 44563 (2017).
[28] T. M. Geislinger, B. Eggart, S. Braunmüller, L. Schmid, and T. Franke, Appl. Phys. Lett. **100**, 183701 (2012).
[29] K. Zeming, T. Salafi, C. Chen, and Y. Zhang, Scientific Reports **6**, 22934 (2016).
[30] D. Holmes, G. Whyte, J. Bailey, N. Vergara-Irigaray, A. Ekpenyong, J. Guck, and T. Duke, Interface Focus **4**, 20140011 (2014).
[31] O. Aouane, M. Thiébaud, A. Benyoussef, C. Wagner, and C. Misbah, Phys. Rev. E **90**, 033011 (2014).
[32] H. Li and G. Ma, Phys. Rev. E **82**, 026304 (2010).
[33] D. S. Hariprasad and T. W. Secomb, Phys. Rev. E **92**, 033008 (2015).
[34] A. Guckenberger, A. Kihm, T. John, C. Wagner, and S. Gekle, Soft Matter **14**, 2032 (2018).
[35] A. Nait-Ouhra, A. Guckenberger, A. Farutin, H. Ez-Zahraouy, A. Benyoussef, S. Gekle, and C. Misbah, Phys. Rev. Fluids **3**, 123601 (2018).
[36] C. E. McLaren, G. M. Brittenham, and V. Hasselblad, American Journal of Physiology-Heart and Circulatory Physiology **252**, H857 (1987).
[37] S. Meßlinger, B. Schmidt, H. Noguchi, and G. Gompper, Phys. Rev. E **80**, 011901 (2009).
[38] S. Sukumaran and U. Seifert, Phys. Rev. E **64**, 011916 (2001).
[39] H. Zhao, A. P. Spann, and E. S. G. Shaqfeh, Phys. Fluids **23**, 121901 (2011).
[40] A. Farutin and C. Misbah, Phys. Rev. Lett. **110**, 108104 (2013).
[41] N. Callens, C. Minetti, G. Coupier, M. Mader, F. Dubois, C. Misbah, and T. Podgorski, Europhys. Lett. **83**, 24002 (2008).
[42] L. Bureau, G. Coupier, F. Dubois, A. Duperray, A. Farutin, C. Minetti, C. Misbah, T. Podgorski, D. Tsvirkun, and M. Vysokikh, C. R. Mécanique **345**, 78 (2017).
[43] M. Abkarian, C. Lartigue, and A. Viallat, Phys. Rev. Lett. **88**, 068103 (2002).
[44] S. Nix, Y. Imai, D. Matsunaga, T. Yamaguchi, and T. Ishikawa, Phys. Rev. E **90**, 043009 (2014).
[45] R. K. Singh, X. Li, and K. Sarkar, Journal of Fluid Mechanics **739**, 421443 (2014).
[46] D. Morris and A. Williams, Biochimica et Biophysica Acta (BBA) - Biomembranes **550**, 288 (1979).
[47] H. L. Goldsmith and J. Marlow, Proc. R. Soc. B **182**, 351 (1972).
[48] M. Bitbol, Biophys. J. **49**, 1055 (1986).
[49] L. Lanotte, J. Mauer, S. Mendez, D. A. Fedosov, J.-M. Fromental, V. Claveria, F. Nicoud, G. Gompper, and M. Abkarian, Proceedings of the National Academy of Sciences **113**, 13289 (2016).
[50] C. Minetti, V. Audemar, T. Podgorski, and G. Coupier, Journal of Fluid Mechanics **864**, 408448 (2019).
[51] X. Grandchamp, G. Coupier, A. Srivastav, C. Minetti, and T. Podgorski, Phys. Rev. Lett. **110**, 108101 (2013).
[52] B. Kaoui, G. Ristow, I. Cantat, C. Misbah, and W. Zimmermann, Phys. Rev. E **77**, 021903 (2008).
[53] G. Danker, P. M. Vlahovska, and C. Misbah, Phys. Rev. Lett. **102**, 148102 (2009).
[54] G. Coupier, B. Kaoui, T. Podgorski, and C. Misbah, Phys. Fluids **20**, 111702 (2008).
[55] T. M. Geislinger and T. Franke, Advances in Colloid and Interface Science **208**, 161 (2014).
[56] S. Roman, S. Lorthois, P. Duru, and F. Risso, Microvasc. Res. **84**, 249 (2012).
[57] J. S. Lawrence, Journal of Clinical Pathology **3**, 332 (1950).
[58] G. Bradski, Dr. Dobb's Journal of Software Tools (2000).
[59] L. Pasol, M. Martin, M. Ekiel-Jeewska, E. Wajnryb, J. Bawzdziewicz, and F. Feuillebois, Chemical Engineering Science **66**, 4078 (2011).
[60] H. Bruus, *Theorical microfluidics* (Oxford University Press, USA, 2008) p. 346.
[61] A. Goldman, R. Cox, and H. Brenner, Chemical Engineering Science **22**, 637 (1967).
[62] K. Sinha and M. D. Graham, Phys. Rev. E **92**, 042710 (2015).
[63] R. Storn and K. Price, Journal of Global Optimization **11**, 341 (1997).
[64] S. Piomelli and C. Seaman, American Journal of Hematology **42**, 46 (1993).
[65] V. Bocci, British Journal of Haematology **48**, 515 (1981).
[66] R. Waugh, M. Narla, C. Jackson, T. Mueller, T. Suzuki, and G. Dale, Blood **79**, 1351 (1992).
[67] O. Linderkamp and H. Meiselman, Blood **59**, 1121 (1982).

[68] G. Deplaine, I. Safeukui, F. Jeddi, F. Lacoste, V. Brousse, S. Perrot, S. Biligui, M. Guillotte, C. Guitton, S. Dokmak, B. Aussilhou, A. Sauvanet, D. Cazals Hatem, F. Paye, M. Thellier, D. Mazier, G. Milon, N. Mohandas, O. Mercereau-Puijalon, P. H. David, and P. A. Buffet, Blood **117**, e88 (2011).

[69] J. Sosa, N. Nielsen, S. Vignes, T. Chen, and S. Shevkoplyas, Clinical Hemorheology and Microcirculation **57**, 275 (2014).

[70] B. Kaoui, G. Coupier, C. Misbah, and T. Podgorski, Houille Blanche **5**, 112 (2009).

[71] S. Nix, Y. Imai, and T. Ishikawa, J. Biomech. **49**, 2249 (2016).

[72] L. Risser, F. Plouraboué, P. Cloetens, and C. Fonta, Int. J. Dev. Neurosci. **27**, 185 (2009).

[73] M. Peyrounette, Y. Davit, M. Quintard, and S. Lorthois, PLoS one **13**, 1 (2018).